PAPER

Surface plasmon coupling regulated CsPbBr₃ perovskite lasers in a metal–insulator–semiconductor structure†

Maogao Gong,‡[a] Di Jiang,‡[a] Tao Tao,[a] Feng Chen, [iD] *[b] Chunxiang Xu, [iD] *[c] Ting Zhi,[d] Wei Liu,[e] Bin Liu,*[a] Rong Zhang[a] and Youdou Zheng[a]

A strong coupling effect often occurs between a metal and semiconductor, so micro/nano-lasers based on surface plasmons can break through the optical diffraction limit and realize unprecedented linear and nonlinear enhancement of optical processes. Hence, metal–insulator–semiconductor (M–I–S) structures based on perovskite materials were explored to design optoelectronic devices. Herein, we constructed an Ag/SiO₂/CsPbBr₃ hybrid structure to generate surface plasmon coupled emission between the metal and CsPbBr₃ perovskite. Combined with experimental characterization and COMSOL Multiphysics software simulations, the best enhancement for CsPbBr₃ radiative recombination efficiencies can be achieved with a 10 nm-thickness of the SiO₂ layer and 80 nm-thickness of the Ag metal film, further verified by optimizing the thickness of the SiO₂ layer above the Ag metal film. In this state, the laser threshold can be as low as 0.138 μW with a quality (Q) factor of up to 3907 under optical pumping, which demonstrate a significant step toward practical applications in biological technology, chemical identification, and optical interconnections of information transmission.

Introduction

Nowadays, the emerging trihalide perovskite materials are considered as promising candidates to achieve high quality micro/nanoscale lasing devices and have attracted tremendous attention from researchers, mainly benefitting from their outstanding characteristics, such as high photoluminescence (PL) quantum yields (~100%), narrow emission bandwidths, long charge-diffusion length, high absorption coefficient, low-cost fabrication routes, and so on.[1–9] Owing to these salient features, the development of high-quality perovskite lasers with tunable emission wavelength has accelerated quickly through intensive research efforts in the past decades,[10–13] and they were realized successfully using Fabry–Pérot (F–P) and whispering gallery mode (WGM) resonators based on single crystals of micro-nanostructured perovskites and applied in various fields, such as high-density data storage, large-scale optoelectronic integration, and high-resolution optical imaging.[14–17] Afterwards, with the development of materials and technology, the laser research hotspot turns gradually to focus in the direction of smaller volume, higher power, higher efficiency, and faster modulation speed. And more and more attention was devoted to the coupling paths through metal–insulator layers with perovskite materials to generate surface plasmon resonance, which could break optical diffraction limit and enhance plasmon coupling efficiency compared to conventional semiconductor lasers, even though when their physical dimension and optical mode volume were scaled down to the sub-wavelength range.[18–20] In 2003, the concept of surface plasmon amplification by stimulated emission of radiation (SPASER) was proposed by M. I. Stockman and D. J. Bergman, as a promising method for shrinking the lasing device to the nanoscale.[21–23] Subsequently, various plasmons with perovskite resonant cavities were triggered explosive development and investigated drastically.[24–28] For example, Cheng *et al.* conducted in full-spectrum modeling that featured hybrid perovskite nanowires placed on different SiO₂-coated metallic (Au, Ag, and Al) plates, the corresponding experimental results for the MAPbBr₃ nanolaser on Ag revealed the low-threshold operation at approximately 1.62 μW average power.[29] In addition, Yu *et al.*

[a] Jiangsu Provincial Key Laboratory of Advanced Photonic and Electronic Materials, School of Electronic Science and Engineering, Nanjing National Laboratory of Microstructures, Nanjing University, Nanjing 210093, P. R. China. E-mail: bliu@nju.edu.cn

[b] School of Physical and Mathematical Sciences, Nanjing Tech University, Nanjing 211800, P. R. China. E-mail: fengchenzql@njtech.edu.cn

[c] State Key Laboratory of Bioelectronics, School of Biological Sciences and Medical Engineering, Southeast University, Nanjing 210096, P. R. China. E-mail: xcxseu@seu.edu.cn

[d] School of Electronic Science and Engineering, Nanjing University of Posts and Telecommunications, Nanjing 210023, P. R. China

[e] College of Optical, Mechanical and Electrical Engineering, Zhejiang A&F University, Hangzhou 311300, P. R. China

† Electronic supplementary information (ESI) available. See DOI: 10.1039/d1ra06828h

‡ Maogao Gong and Di Jiang contributed equally to this work.

demonstrated plasmonic laser action using a hybrid geometry whereby the MAPbI$_3$ perovskite nanowires were placed on an Ag substrate with an insulating spacer layer. Relatively low threshold operation under ambient condition (13.5 μJ cm^{-2}) was reported, and the device could work well even at temperatures up to 43.6 °C. However, as is known to all, using organic–inorganic hybrid perovskites as high gain medium still exists several issues, mainly due to their physical and chemical stability are poor compared to all-inorganic perovskite materials when exposed to environments under heat and humidity conditions.[30,31] At the moment, the newly developed all-inorganic perovskite materials (CsPbX$_3$, X = Cl, Br, I) exhibit unprecedented light harvesting and light-emitting properties in the field of small laser devices. In especial, CsPbBr$_3$ perovskite materials stand out and display remarkable characteristics, owing to their highly improved optical performance and thermal stability, high quantum yield, and low trap state density, which enable them to be the promising alternative materials for realizing low-threshold plasmonic lasers, where high optical gain is essential. In 2016, Eaton et al. first reported the application of all-inorganic perovskite nanowires in the laser field.[32] They prepared CsPbBr$_3$ and CsPbCl$_3$ nanowires successfully by the liquid-phase cryogenic solution method and used them as gain media. Under pulsed laser excitation, the lasing threshold of CsPbBr$_3$ nanowires was 5 μJ cm^{-2}, and the maximum quality factor was about 1009. Meanwhile, the experimental results provided evidence for the correctness of the electron–hole plasma mechanism. Compared with the previously reported organic–inorganic hybrid perovskite, all-inorganic perovskite exhibited better stability. Lasing under constant, pulsed excitation can be maintained for over 1 h, the equivalent of 10^9 excitation cycle.[33]

Experimental section

In this work, the CsPbBr$_3$ perovskite samples were obtained by using the anti-solvent crystallization technique. 0.2 M of CsBr and a PbBr$_2$ solution were mixed together with a volume ratio of 1 : 1 in anhydrous N,N-dimethylformamide (DMF) and then gently shaken until their complete dissolution, and formed CsPbBr$_3$ crystals with desirable diffusion eventually. Afterwards, the CsPbBr$_3$ solution was dispersed onto a silicon and M–I–S structures, respectively, and sealed in a beaker to control the evaporation rate. After about 24 hours at room temperature, CsPbBr$_3$ micro-cubes were prepared on the substrates. It's noted that the insulator SiO$_2$ thickness in M–I–S structures was designed as 10 nm, 30 nm, and 60 nm between the CsPbBr$_3$ semiconductor and Ag metal layer, and they were marked as sample B, C, and D, severally, while the prepared sample in bare silicon substrate was marked as sample A. Remarkably, M–I–S structures were fabricated successfully using the following steps: Firstly, 200 nm-thickness of SiO$_2$ layer was grown on the Si substrate by plasma enhanced chemical vapor deposition (PECVD). Secondly, 80 nm-thickness of Ag film was placed on the above SiO$_2$ layer by electron beam evaporation. And finally, different thickness of SiO$_2$ layer was grown on Ag film by PECVD to act as the insulator layer. The detailed descriptions were listed in Table 1.

Table 1 The detailed descriptions of four samples

Sample	Substrate	SiO$_2$ thickness	Ag thickness	SiO$_2$ thickness
A	Si			
B	Si	200 nm	80 nm	10 nm
C				30 nm
D				60 nm

The sample's crystal quality was characterized by using an X-ray powder diffractometer (XRD), and scanning electron microscopy (SEM) images and EDX spectra of sample microstructures were obtained by using a Zeiss Gemini 500 field emission scanning electron microscope operated at 5 kV. Focused ion beam (FIB) system was further employed to observe the cross-section area of sample. Meanwhile, a high-resolution transmission electron microscopy (HRTEM) test was carried out using FEI Tecnai G2 F20 S-TWIN device. For optical characterizations, samples were excited using a femtosecond laser at a wavelength of 325 nm (150 fs, 1 kHz) in a micro-photoluminescence system, and the PL spectra were collected by using a spectrometer (Spectra Pro-2500i, Acton Research Corporation). Time-resolved PL (TRPL) measurements were carried out by utilizing a streak camera (Optronis Optoscope sc-10). All measurements were executed at room temperature.

Results and discussion

Fig. 1(a) demonstrates the crystal structure diagram of CsPbBr$_3$ perovskite sample, it owns the octahedral geometry. The positive monovalent Cs ion (azury ball) locates within the center of eight lead bromide octahedrons.[34] As shown in Fig. 1(b), CsPbBr$_3$ micro-cube is placed on an Ag/SiO$_2$/CsPbBr$_3$ hybrid structure. When it is pumped by a high power 325 nm femtosecond pulsed laser, here will emit strong green light. As the output power increases steadily, PL intensity increases abruptly at certain value and laser emission phenomenon can appear.

Fig. 2(a)–(d) show SEM images of four CsPbBr$_3$ samples, respectively. It is found that the CsPbBr$_3$ micro-cubes own very smooth surfaces and exhibit different morphology features and sizes, such as regular cube and cuboid shapes, and dimensions
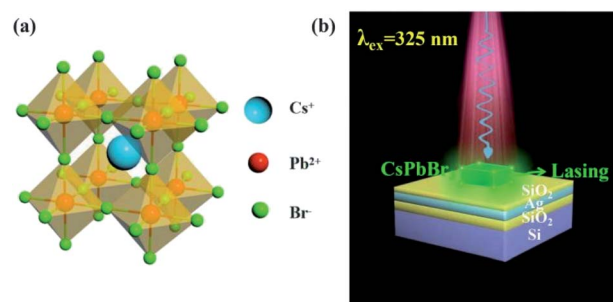

Fig. 1 (a) Crystal structure diagram of CsPbBr$_3$ perovskite material; (b) schematic of a CsPbBr$_3$ micro-cube on a surface plasmon substrate pumped by a 325 nm femtosecond pulsed laser.
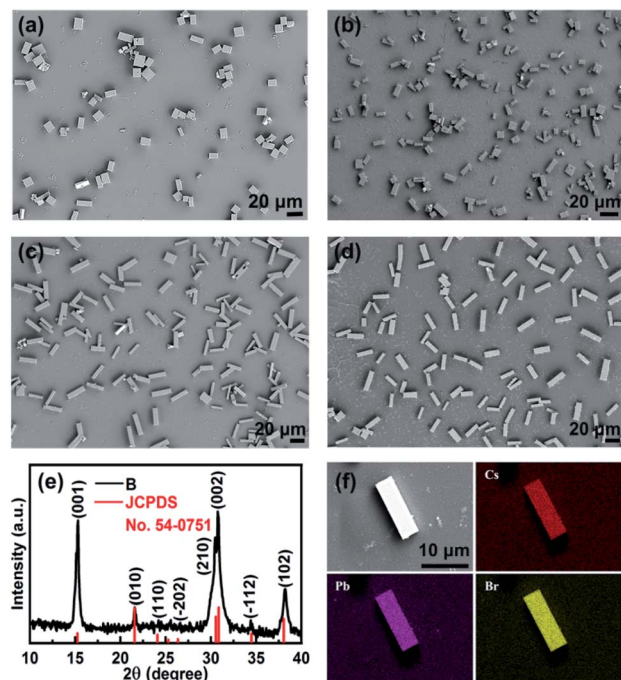
Fig. 2 (a–d) SEM images of the as-obtained four samples, respectively; (e) XRD pattern of sample B; (f) the EDS elemental mapping for sample B.
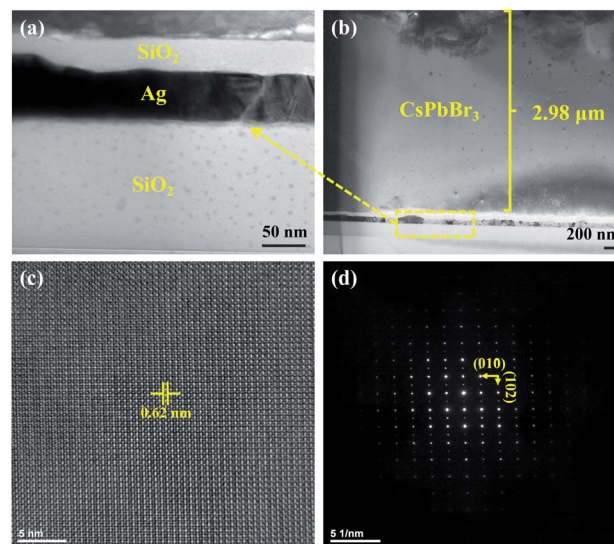

Fig. 3 (a and b) Cross-sectional SEM images; (c) HRTEM image; and (d) selective-area electron diffraction (SAED) image of the as-obtained sample D, respectively.

range from a few microns to dozens of microns, further indicating that the various morphology and sizes of CsPbBr$_3$ samples can be prepared successfully. The crystal pattern and quality of CsPbBr$_3$ samples continue to be detected. The XRD characterization was conducted in Fig. 2(e). The sharp peaks measured from sample B are consistent with the standard card JCPDS No. 54-0751 of CsPbBr$_3$ crystal. And EDS elemental mapping was displayed in Fig. 2(f); the atomic ratio of Br/Pb is estimated to be 3 : 1. The mapping of elements can confirm the presence of Cs, Pb, and Br elements and uniform distribution in the micro-cube. All of these XRD, SEM, and EDS results demonstrate the high crystalline quality of acquired CsPbBr$_3$ samples.

To further investigate the Ag/SiO$_2$/CsPbBr$_3$ hybrid structure, FIB-SEM test was carried out to character their cross-sections. The cross-sectional FESEM images of remaining samples B and C with varying layer thicknesses have been provided in Fig. S1.† Fig. 3(a) and (b) exhibit clear substrate and CsPbBr$_3$ profiles of each layer interface. And the thickness of each layer can match well with our previous designed goal in Table 1. The thickness of CsPbBr$_3$ perovskite layer above the M–I–S structure is about 2.98 μm. Furthermore, the corresponding HRTEM and SAED analyses were presented in Fig. 3(c) and (d), evidencing that the distinct lattice fringes are very regular and arrange orderly, the lattice distance is about 0.62 nm, which demonstrates the high crystalline quality of as-obtained sample D. More significantly, the crystal planes of (010) and (102) are consistent with XRD test in Fig. 2(e).

The lasing actions were investigated shown in Fig. 4. As displayed in Fig. 4(a), the PL intensity will increase quickly as

the pump power increases from 23 μW to 140 μW. However, laser emission behavior is not observed, maybe due to the laser gain is not sufficient for sample A. By contrast, the typical single-mode lasing behaviors from CsPbBr$_3$ micro-cubes can be achieved successfully, and the PL intensity increases abruptly when the output laser power increases to a certain value, which triggers off the laser emission behavior. Meanwhile, the ultra-low laser threshold is obtained and increases from 0.138 μW to 2.586 μW shown in Fig. 4(e)–(g), and the FWHM value can reach the minimum value of 0.14 nm for sample B with the laser emission wavelength at 547 nm. A high Q-factor of 3907 is calculated through the equation as follows shown in Fig. 4(h). As the insulator layer thickness increases, the lasing threshold increases, and Q decreases inversely. The optimized condition is 10 nm thickness of SiO$_2$ layer above 80 nm thickness of Ag metal film just as mentioned before. Furthermore, the thinner below 10 nm or none SiO$_2$ layer will make Ag metal film easier to
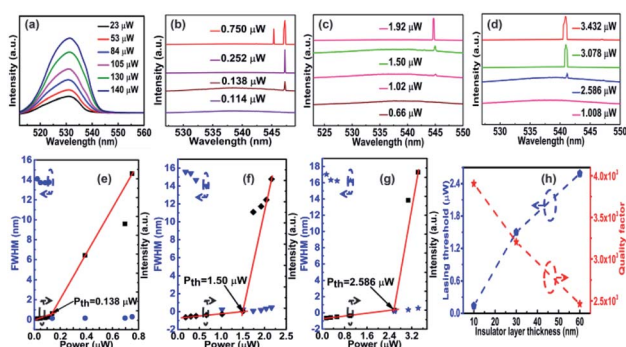

Fig. 4 Power dependent PL spectra of samples A (a), B (b), C (c), and D (d); (e–g) PL intensity and FWHM values from CsPbBr$_3$ micro-cubes as a function of pump power; (h) lasing threshold and Q as a function of insulator layer thickness, respectively.

oxidize, further resulting in generating material defects, increasing surface roughness, and improving the Ohm loss that affects the confinement of the electric field between CsPbBr$_3$ perovskite and Ag metal film. This will supply an arena to boost the optoelectronic and laser applications of CsPbBr$_3$ samples with high performance. Moreover, the acquisition of ultralow-threshold laser with CsPbBr$_3$ perovskite is mainly ascribed to the well-designed M–I–S structure and high optical gain material, which can induce to generate strong exciton–photon coupling effect and increase the refractive index.[18,35]

$$Q = \lambda/\delta\lambda \qquad (1)$$

where λ and $\delta\lambda$ are the lasing mode wavelength and its FWHM, respectively.

The streak camera images of sample B below (Fig. 5(a)) and above (Fig. 5(b)) the lasing threshold were used to study the carrier population dynamics for CsPbBr$_3$-based laser cavity, and the emergence of a rapid decay component suggested fast carrier radiative recombination rate due to stimulated emission. In addition, as shown in Fig. 5(c), a standard two-exponential-component model was used to fit the decay traces.[36,37]

$$y = A_1 \exp(-t/\tau_1) + A_2 \exp(-t/\tau_2) \qquad (2)$$

where A_1 and A_2 are constants, τ_1 and τ_2 are the fast and slow components of PL lifetime, respectively. Results exhibit that the carriers of CsPbBr$_3$ micro-cubes grown on M–I–S structures radiate faster than those in the bare Si substrate. Meanwhile, as the insulator layer SiO$_2$ thickness increases, the decay time τ_1 and τ_2 increase from 49.93 picosecond (ps) to 61.98 ps and from 288.02 ps to 356.45 ps, respectively. The fast decay rates illustrate that additional recombination channels for CsPbBr$_3$ micro-cubes are established *via* using M–I–S structures, verifying that the effect of M–I–S structures is prominent. And the carrier recombination rate of sample B is faster than others, which proves that it owns the optimal performance among them currently.

The simulated electric field distributions of four samples have been carried out to study using COMSOL Multiphysics software as shown in Fig. 6. The result demonstrates that the electric field distribution is dispersive and hard to localize for sample A in Fig. 6(a). By contrast, the localization effect of electric field becomes intensive and concentrates on the location between the Ag metal layer and CsPbBr$_3$ perovskite. And the maximum electric field intensity value in the microlaser structure decreases from 6.32 V m^{-1} to 3.06 V m^{-1} with increasing the insulator layer SiO$_2$ thickness in Fig. 6(b)–(d), proving that the M–I–S structures can indeed improve the photons of incident light and enhance exciton–photon coupling effect compared with bare Si substrate structure. Moreover, the conclusions of theoretical simulation are very consistent with experimental results as above. However, as the thickness of SiO$_2$ layer increases to 60 nm or over, the electric field intensity value for sample D approaches to sample A (2.87 V m^{-1}), which exhibits that the effect of M–I–S structure begins to become unconspicuous gradually, attributing to that the thickness of SiO$_2$ layer is too thick to trigger the plasmon resonance action. In this situation, it looks that the SiO$_2$ layer should be as thin as possible or even none to obtain stronger exciton–photon coupling effect. It is not the case, if the SiO$_2$ layer is too thin or none, the electric field density increases rapidly, but the metal loss also becomes serious and the lasing modes are unstable as well.[18] Referring to our previously published literature,[20] the surface plasmon resonance mechanism between CsPbBr$_3$ perovskite and Ag metal film was depicted. It can be found that a large population of excitons is initially excited. Benefiting from existing a near field coupling between the excitons and surface plasmons, here can generate plasmon–exciton-polaritons, which induces relevant quasiparticles in the CsPbBr$_3$-based perovskite laser. Those polaritons then radiate coherently *via* stimulated relaxation into the plasmonic lasing modes, further providing a faster radiation tunnel by the following expression:[38]

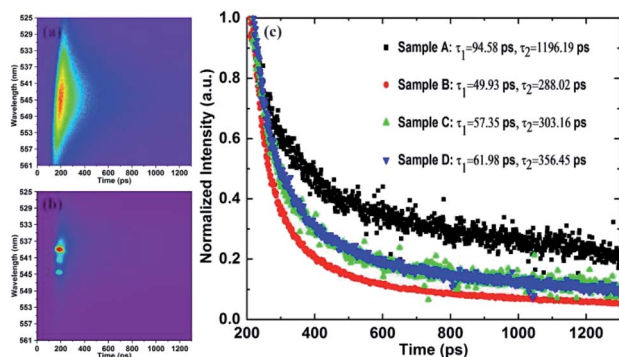$$1/\tau_{coupled} = 1/\tau_{nr} + 1/\tau_r + 1/\tau_{sp} \approx 1/\tau_{sp} \qquad (3)$$

Fig. 5 Streak camera images of sample B below (a) and above (b) the lasing threshold; (c) the decay traces of four CsPbBr$_3$ samples with detection wavelength fixed at each PL peak.
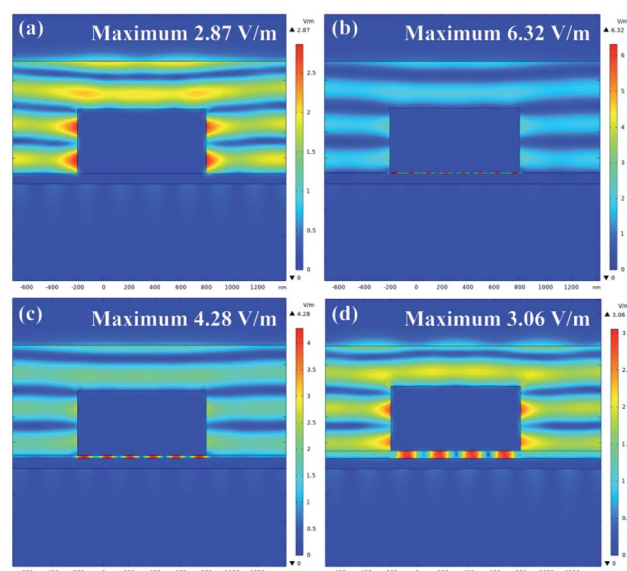

Fig. 6 Simulated electric field distributions and the maximum electric field intensity values of sample (a) A, (b) B, (c) C, and (d) D, respectively.

The experimentally determined $\tau_{coupled}$ can be described as a Purcell-enhanced spontaneous emission rate (F/τ_r), where F is the enhancement factor by the Purcell effect.[39–43] Purcell effect increases the fraction of polaritons in the plasmonic lasing mode, yielding a lower laser threshold eventually.[44–51]

Conclusions

In summary, the structures of metal–insulator layers combined with $CsPbBr_3$ perovskite materials were investigated successfully. And results reveal that the thickness of insulator layer of SiO_2 and substrate can affect laser generation. Theoretical and experimental results prove that the as-obtained sample B with the thickness of 10 nm SiO_2 layer and 80 nm Ag metal film, demonstrates a ultra-low laser threshold as low as 0.138 μW and a high quality (Q) factor of up to 3907, which exhibits the excellent performance compared with the previous reported $CsPbBr_3$ perovskite lasers. It paves the way for the development of high-efficiency $CsPbBr_3$-based micro/nano-lasers and provides fundamental insights for the practical applications of all-inorganic $CsPbBr_3$ perovskite micro-cubes in biomedical, data storage, and on-chip optical communication technologies in the future.

Conflicts of interest

The authors declare no competing financial interests.

Acknowledgements

References

1 R. E. Beal, D. J. Slotcavage, T. Leijtens, A. R. Bowring, R. A. Belisle, W. H. Nguyen, G. F. Burkhard, E. T. Hoke and M. D. McGehee, Cesium Lead Halide Perovskites with Improved Stability for Tandem Solar Cells, *J. Phys. Chem. Lett.*, 2016, 7, 746–751.

2 A. Schlaus, M. Spencer, K. Miyata, F. Liu, X. X. Wang, I. Datta, M. Lipson, A. L. Pan and X. Y. Zhu, How Lasing Happens in $CsPbBr_3$ Perovskite Nanowires, *Nat. Commun.*, 2019, 10, 265.

3 X. Wang, H. Zhou, S. Yuan, W. Zheng, Y. Jiang, X. Zhuang, H. Liu, Q. Zhang, X. Zhu, X. Wang and A. L. Pan, Cesium Lead Halide Perovskite Triangular Nanorods as High-Gain Medium and Effective Cavities for Multiphoton-Pumped Lasing, *Nano Res.*, 2017, 10, 3385–3395.

4 Q. Zhang, R. Su, X. Liu, J. Xing, T. C. Sum and Q. H. Xiong, High Quality Whispering-Gallery-Mode Lasing from Cesium Lead Halide Perovskite Nanoplatelets, *Adv. Funct. Mater.*, 2016, 26, 6238–6245.

5 Y. Wang, X. Sun, R. Shivanna, Y. Yang, Z. Chen, Y. Guo, G. C. Wang, E. Wertz, F. Deschler and Z. Cai, Photon Transport in One-Dimensional Incommensurately Epitaxial $CsPbX_3$ Arrays, *Nano Lett.*, 2016, 16, 7974.

6 J. Chen, Y. Fu, L. Samad, L. Dang, Y. Zhao, S. Shen, L. Guo and J. Song, Vapor-Phase Epitaxial Growth of Aligned Nanowire Networks of Cesium Lead Halide Perovskites ($CsPbX_3$, X = Cl, Br, I), *Nano Lett.*, 2017, 17, 460.

7 F. Chen, C. X. Xu, Q. Y. Xu, Z. Zhu, F. F. Qin, A. Gowri Manohari and Y. Z. Zhu, Lasing mode evolution and regulation of the perovskite $CH_3NH_3PbBr_3$, *J. Mater. Chem. C*, 2017, 5, 9238–9241.

8 Z. Z. Liu, J. Yang, J. Du, Z. P. Hu, T. C. Shi, Z. Y. Zhang, Y. Q. Liu, X. S. Tang, Y. X. Leng and R. X. Li, Robust Subwavelength Single-Mode Perovskite Nanocuboid Laser, *ACS Nano*, 2018, 12, 5923–5931.

9 F. Chen, C. Zhu, C. X. Xu, P. Fan, F. F. Qin, A. Gowri Manohari, J. F. Lu, Z. L. Shi, Q. Y. Xu and A. L. Pan, Crystal structure and electron transition underlying photoluminescence of methylammonium lead bromide perovskites, *J. Mater. Chem. C*, 2017, 5, 7739–7745.

10 B. E. Zhou, M. M. Jiang, H. X. Dong, W. H. Zheng, Y. Z. Huang, J. Y. Han, A. L. Pan and L. Zhang, High-Temperature Upconverted Single-Mode Lasing in 3D Fully Inorganic Perovskite Microcubic Cavity, *ACS Photonics*, 2019, 6, 793–801.

11 X. X. Wang, M. Shoaib, X. Wang, X. H. Zhang, M. He, Z. Y. Luo, W. H. Zheng, H. L. Li, T. F. Yang, X. L. Zhu, L. B. Ma and A. L. Pan, High-Quality In-Plane Aligned $CsPbX_3$ Perovskite Nanowire Lasers with Composition-Dependent Strong Exciton-Photon Coupling, *ACS Nano*, 2018, 12, 6170–6178.

12 Y. G. Zhong, K. Liao, W. N. Du, J. R. Zhu, Q. Y. Shang, F. Zhou, X. X. Wu, X. Y. Sui, J. W. Shi, S. Yue, Q. Wang, Y. F. Zhang, Q. Zhang, X. Y. Hu and X. F. Liu, Large-Scale Thin $CsPbBr_3$ Single-Crystal Film Grown on Sapphire *via* Chemical Vapor Deposition: Toward Laser Array Application, *ACS Nano*, 2020, 14, 15605–15615.

13 R. Chen, B. Ling, X. W. Sun and H. D. Sun, Room Temperature Excitonic Whispering Gallery Mode Lasing from High-Quality Hexagonal ZnO Microdisks, *Adv. Mater.*, 2011, 23, 2199–2204.

14 J. C. Johnson, H. J. Choi, K. P. Knutsen, R. D. Schaller, P. Yang and R. J. Saykally, Single Gallium Nitride Nanowire Lasers, *Nat. Mater.*, 2002, 1, 106–110.

15 C. Czekalla, C. Sturm, R. Schmidt-Grund, B. Cao, M. Lorenz and M. Grundmann, Whispering Gallery Mode Lasing in Zinc Oxide Microwires, *Appl. Phys. Lett.*, 2008, 92, 241102.

16 M. H. Huang, S. Mao, H. Feick, H. Yan, Y. Wu, H. Kind, E. Weber, R. Russo and P. Yang, Room-Temperature Ultraviolet Nanowire Nanolasers, *Science*, 2001, 292, 1897–1899.

© 2021 The Author(s). Published by the Royal Society of Chemistry

17 M. S. Gudiksen, L. J. Lauhon, J. Wang, D. C. Smith and C. M. Lieber, Growth of Nanowire Superlattice Structures for Nanoscale Photonics and Electronics, *Nature*, 2002, **415**, 617–620.

18 D. Jiang, B. Liu, T. Tao, T. Zhi, P. Chen, D. J. Chen, Z. L. Xie, X. Q. Xiu, Y. D. Zheng and R. Zhang, The optimization of surface plasmon coupling efficiency in InGaN/GaN nanowire based nanolasers, *Appl. Phys. Express*, 2020, **13**, 085001.

19 T. Tao, T. Zhi, B. Liu, J. P. Dai, Z. Zhuang, Z. L. Xie, P. Chen, F. F. Ren, D. J. Chen, Y. D. Zheng and R. Zhang, Manipulable and Hybridized, Ultralow-Threshold Lasing in a Plasmonic Laser Using Elliptical InGaN/GaN Nanorods, *Adv. Funct. Mater.*, 2017, **27**, 1703198.

20 T. Tao, T. Zhi, B. Liu, P. Chen, Z. L. Xie, H. Zhao, F. F. Ren, D. J. Chen, Y. D. Zheng and R. Zhang, Electron-Beam-Driven III-Nitride Plasmonic Nanolasers in the Deep-UV and Visible Region, *Small*, 2020, **16**, 1906205.

21 R. F. Oulton, V. J. Sorger, D. A. Genov, D. F. P. Pile and X. Zhang, A hybrid plasmonic waveguide for subwavelength confinement and long-range propagation, *Nat. Photonics*, 2008, **2**, 496.

22 R. F. Oulton, V. J. Sorger, T. Zentgraf, R. M. Ma, C. Gladden, L. Dai, G. Bartal and X. Zhang, Plasmon lasers at deep subwavelength scale, *Nature*, 2009, **461**, 629.

23 M. I. Stockman and D. J. Bergman, Quantum nanoplasmonics: surface plasmon amplification by stimulated emission of radiation (SPASER), *Quantum Electronics & Laser Science. QELS Postconference Digest IEEE*, 2003.

24 R. M. Ma and R. F. Oulton, Applications of nanolasers, *Nat. Nanotechnol.*, 2019, **14**, 12.

25 M. A. Noginov, G. Zhu, A. M. Belgrave, R. Bakker, V. M. Shalaev, E. E. Narimanov, S. Stout, E. Herz, T. Suteewong and U. Wiesner, Demonstration of a spaser-based nanolaser, *Nature*, 2009, **460**, 1110.

26 R. M. Ma, R. F. Oulton, V. J. Sorger, G. Bartal and X. Zhang, Room-temperature sub-diffraction-limited plasmon laser by total internal reflection, *Nat. Mater.*, 2011, **10**, 110.

27 S. Arafin, X. Liu and Z. Mi, Review of recent progress of III-nitride nanowire lasers, *J. Nanophotonics*, 2013, **7**, 074599.

28 Z. Han and S. I. Bozhevolnyi, Radiation guiding with surface plasmon polaritons, *Rep. Prog. Phys.*, 2013, **76**, 016402.

29 P. J. Cheng, Q. Y. Zheng, C. Y. Hsu, H. Li, K. B. Hong, Y. Z. Zhu, Q. N. Cui, C. X. Xu, T. C. Lu and T. R. Lin, Full-Spectrum Analysis of Perovskite-Based Surface Plasmon Nanolasers, *Nanoscale Res. Lett.*, 2020, **15**, 66.

30 H. C. Yu, K. K. Ren, Q. Wu, J. Wang, J. Lin, Z. J. Wang, J. J. Xu, R. F. Oulton, S. C. Qu and P. Jin, Organic-inorganic perovskite plasmonic nanowire lasers with a low threshold and a good thermal stability, *Nanoscale*, 2016, **8**, 19536–19540.

31 Q. Y. Shang, Y. Zhang, Z. Liu, J. Chen, P. F. Yang, C. Li, W. Li, Y. F. Zhang, Q. H. Xiong, X. F. Liu and Q. Zhang, Surface Plasmon Enhanced Strong Exciton-Photon Coupling in Hybrid Inorganic-Organic Perovskite Nanowires, *Nano Lett.*, 2018, **18**, 3335–3343.

32 S. W. Eaton, M. Lai, N. A. Gibson, A. B. Wong, L. Dou, J. Ma, L. W. Wang, S. R. Leone and P. Yang, Lasing in robust cesium lead halide perovskite nanowires, *Proc. Natl. Acad. Sci. U. S. A.*, 2016, **113**, 1993–1998.

33 H. Zhu, Y. Fu, F. Meng, X. Wu, Z. Gong, Q. Ding, M. V. Gustafsson, M. T. Trinh and X. Y. Zhu, Lead halide perovskite nanowire lasers with low lasing thresholds and high quality factors, *Nat. Mater.*, 2015, **14**, 636–642.

34 S. T. Ha, X. F. Liu, Q. Zhang, D. Giovanni, T. C. Sum and Q. H. Xiong, Synthesis of Organic-Inorganic Lead Halide Perovskite Nanoplatelets: Towards High-Performance Perovskite Solar Cells and Optoelectronic Devices, *Adv. Opt. Mater.*, 2014, **2**, 838–844.

35 Q. Y. Shang, M. L. Li, L. Y. Zhao, D. W. Chen, S. Zhang, S. L. Chen, P. Gao, C. Shen, J. Xing, G. C. Xing, B. Shen, X. F. Liu and Q. Zhang, Role of the Exciton-Polariton in a Continuous-Wave Optically Pumped $CsPbBr_3$ Perovskite Laser, *Nano Lett.*, 2020, **20**, 6636–6643.

36 L. Pei, J. S. Zhong, T. Z. Li, W. F. Bai, S. T. Wu, Y. J. Yuan, Y. F. Chen, Z. T. Yu, S. C. Yan and Z. G. Zou, CoS_2@N-doped carbon core-shell nanorod array grown on Ni foam for enhanced electrocatalytic water oxidation, *J. Mater. Chem. A*, 2020, **8**, 6795–6803.

37 Z. Liu, Q. Y. Shang, C. Li, L. Y. Zhao, Y. Gao, Q. Li, J. Chen, S. Zhang, X. F. Liu, Y. S. Fu and Q. Zhang, Temperature-dependent photoluminescence and lasing properties of $CsPbBr_3$ nanowires, *Appl. Phys. Lett.*, 2019, **114**, 101902.

38 A. Yang, T. B. Hoang, M. Dridi, C. Deeb, M. H. Mikkelsen, G. C. Schatz and T. W. Odom, Real-time tunable lasing from plasmonic nanocavity arrays, *Nat. Commun.*, 2015, **6**, 6939.

39 R. M. Ma, S. Ota, Y. Li, S. Yang and X. Zhang, Explosives detection in a lasing plasmon nanocavity, *Nat. Nanotechnol.*, 2014, **9**, 600.

40 A. González-Tudela, P. A. Huidobro, L. Martín-Moreno, C. Tejedor and F. J. García-Vidal, Theory of strong coupling between quantum emitters and propagating surface plasmons, *Phys. Rev. Lett.*, 2013, **110**, 126801.

41 D. Sanvitto and S. Kena-Cohen, The road towards polaritonic devices, *Nat. Mater.*, 2016, **15**, 1061–1073.

42 K. Takazawa, J. I. Inoue, K. Mitsuishi and T. Takamasu, Fraction of a millimeter propagation of exciton polaritons in photoexcited nanofibers of organic dye, *Phys. Rev. Lett.*, 2010, **105**, 067401.

43 M. Li, Q. Wei, S. K. Muduli, Q. Xu, N. Mathews, S. G. Mhaisalkar, G. Xing and T. C. Sum, Enhanced Exciton and Photon Confinement in Ruddlesden-Popper Perovskite Microplatelets for Highly Stable Low-Threshold Polarized Lasing, *Adv. Mater.*, 2018, **30**, 1707235.

44 E. M. Purcell, Spontaneous emission probabilities at radio frequencies, *Phys. Rev.*, 1946, **69**, 681.

45 F. L. Wang, Y. D. Yang, Y. Z. Huang, Z. X. Xiao and J. L. Xiao, Single-transverse-mode waveguide-coupled deformed hexagonal resonator microlasers, *Appl. Opt.*, 2018, **57**, 7242–7248.

46 H. R. Yu, X. Cheng, Y. Wang, Y. Liu, K. Rong, Z. Li, Y. Wan, W. Gong, K. Watanabe and T. Taniguchi, Waterproof

Perovskite-Hexagonal Boron Nitride Hybrid Nanolasers with Low Lasing Thresholds and High Operating Temperature, *ACS Photonics*, 2018, **5**, 4520–4528.

47 J. Ren, Y. Gu, D. Zhao, F. Zhang, T. Zhang and Q. Gong, Evanescent-Vacuum-Enhanced Photon-Exciton Coupling and Fluorescence Collection, *Phys. Rev. Lett.*, 2017, **118**, 073604.

48 S. De Liberato, Light-Matter Decoupling in the Deep Strong Coupling Regime: The Breakdown of the Purcell Effect, *Phys. Rev. Lett.*, 2014, **112**, 16401.

49 E. Waks and D. Sridharan, Cavity QED treatment of interactions between a metal nanoparticle and a dipole emitter, *Phys. Rev. A: At., Mol., Opt. Phys.*, 2010, **82**, 043845.

50 T. Byrnes, N. Y. Kim and Y. Yamamoto, Erratum: Exciton-polariton condensates, *Nat. Phys.*, 2014, **10**, 803–813.

51 K. Wang, W. Sun, J. Li, Z. Gu, S. Xiao and Q. Song, Unidirectional Lasing Emissions from $CH_3NH_3PbBr_3$ Perovskite Microdisks, *ACS Photonics*, 2016, **3**, 1125–1130.